Printability of Native Blank Defects and Programmed Defects and Their Stack Structures

Hyuk Joo Kwon*[a], Jenah Harris-Jones[a], Ranganath Teki[a], Aaron Cordes[a],
Toshio Nakajima[b], Iacopo Mochi[c], Kenneth A. Goldberg[c], Yuya Yamaguchi[d], Hiroo Kinoshita[d]
[a]SEMATECH, 257 Fuller Road Suite 2200 Albany, NY 12203 USA
[b]AGC Electronics America, 257 Fuller Road Suite 2200 Albany, NY 12203 USA
[c]Center for X-ray Optics, LBNL, 1 Cyclotron Road Berkeley, CA 94720 USA
[d]LASTI, University of Hyogo, 3-1-2 Kouto, Kamigoori, Akou-gun, Hyogo 678-1205, Japan

ABSTRACT

We describe the characterization of native phase defects in the manufacturing of extreme ultraviolet (EUV) mask blanks using the state-of-the-art mask metrology equipment in SEMATECH's Mask Blank Development Center (MBDC). We used commercially available quartz substrates and deposited Mo/Si multilayers on the substrates to characterize phase defects. We also prepared programmed defects of various dimensions using e-beam patterning technology on which multilayers were deposited. Transmission electron microscopy (TEM) was used to study multilayer profile changes, while SEMATECH's actinic inspection tool (AIT) was used to image defects and predict their printability. Defect images at different focal depths of the AIT are correlated to TEM cross sections and atomic force microscopy (AFM) dimensions. The printability of native and programmed defects was also investigated.

Keywords: Defect printability, native defect, programmed defect, AIT, TEM, EUV mask, simplified printability model

1. INTRODUCTION

EUV patterning appears feasible using currently available EUV exposure tools, but some issues must still be solved for production of EUV patterning. Defects in EUV mask blanks are one such major issue, as evidenced by the research focused on defect printability.[1-5] Although the dimensions of defects can be characterized using currently available metrology tools, native phase defects cannot be realistically characterized without knowledge of defect-induced changes in the structure of the deposited multilayer.

Inspection tools are needed to detect phase defects on EUV mask blanks that could possibly print on the wafer. Currently available inspection tools can capture defects on the mask, but they also need to be able to classify possible printable defects. Figure 1 shows currently detectable mask depths. The tools operating at DUV light detect signals from the top few layers, while an AIT operating at 13.5 nm detects signals over 30 bilayers. DUV inspection tools can capture defects in EUV blanks, but they cannot separate defects that will print on the wafer from those that will not. Defect classification for repair and mitigation of printable defects is very difficult using DUV inspection tools; however, if the AIT could get defect information from more multilayer stacks, it may be able to separate printable defects from unprintable defects. If unprintable defects could be eliminated, the defect information could be used for mask pattern shifts to reduce printable defects. We also would have to repair fewer defects if we had a better chance of capturing printable defects using an actinic inspection tool. Being able to detect printable defects on EUV blanks is therefore critical in mask making. The worst scenario for DUV inspection tools would be to catch too many defects, most of which will not print on the wafer and are inconsequential. This kind of inspection system is oversensitive to mask defects and not able to distinguish unprintable defects from those that are printable. Likewise, a DUV inspection tool that is not sensitive enough to catch printable defects poses problems in manufacturing. In short, the industry needs reasonable defect sensitivity and detectability of printable defects.

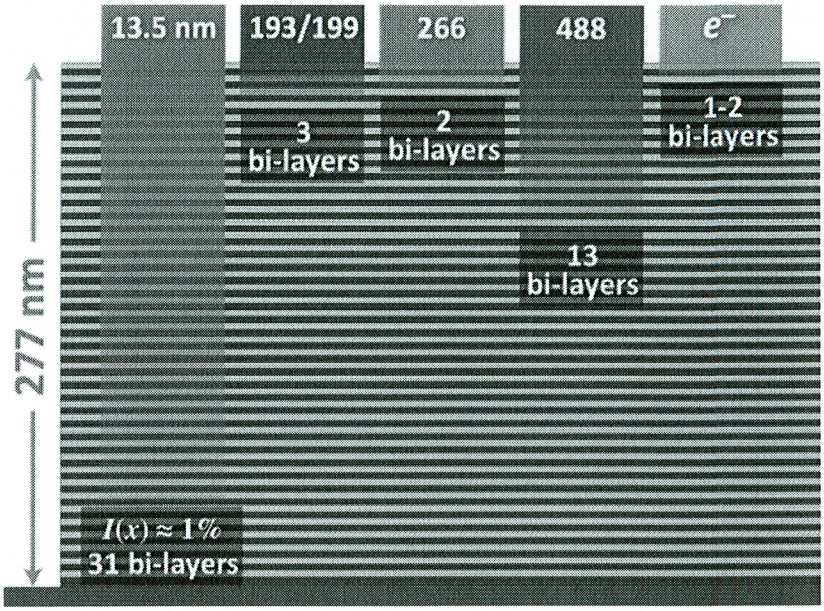

Figure 1. Wavelength for inspection systems and actinic inspection tool.[6]

This paper describes the characterization of native phase defects and programmed defects and analyzes their printability. Defect images in the AIT at different focal depths are correlated to 3D images obtained from SEM, AFM, and TEM. We investigate defect dimensions on the substrate, defect decoration during multilayer deposition, and defect dimensions at the top of the multilayer. The printable and unprintable regions for native defects and programmed defects are compared.

2. EXPERIMENTAL PROCEDURE

Studying the printability of native defects of various dimensions is necessary to determine reasonable defect detection and defect printability parameters. In our study, we investigated printability using both native and programmed defects. Because shapes of native defects have quite abnormal, their dimensions can be difficult to measure. Programmed defects, on the other hand, are relatively easy to characterize because their dimensions are easily defined by conventional e-beam patterning. The printability of both kinds of defects was characterized to correlate unprintable and printable regions with defect dimensions and shapes. The printability characteristics of native and programmed defects were then compared.

2.1 Native defects

The procedure to prepare and evaluate the masks is shown in figure 2. We deposited multilayers on quartz substrates and inspected the plates using the M7360 tool. The native defects captured by the M7360 were measured using AFM and SEM to determine their dimensions. The masks were inspected using SEMATECH's Berkeley AIT after punchmarking 10 μm from the native defects of interest. The numerical aperture (NA) for AIT inspection was 0.35 and the focus range was -200 nm to +200 nm. The AIT-inspected images were analyzed using ThroughFocus analysis software. The masks were then characterized by TEM to analyze after AIT inspection.

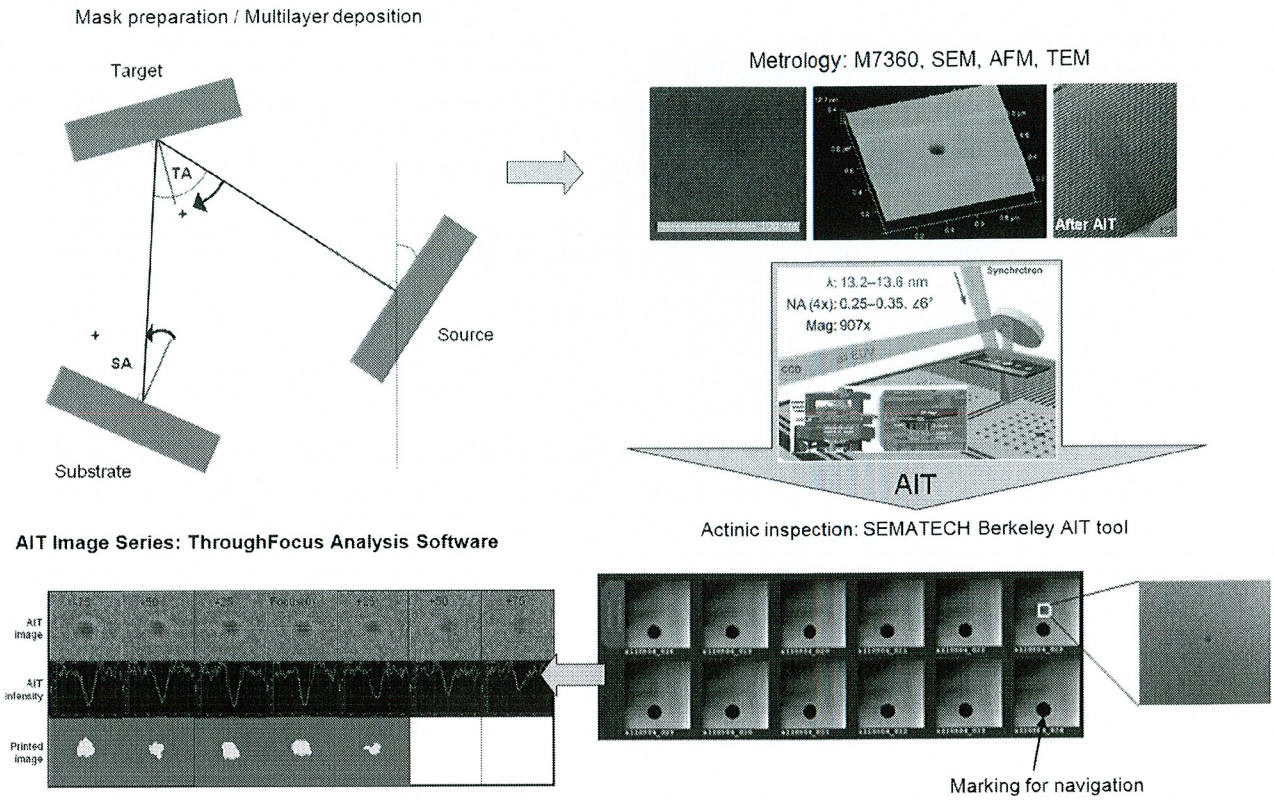

Figure 2. Experimental procedure for mask preparation and defect analysis.

2.2 Programmed defects

Figure 3 shows the procedure to manufacture programmed defects. Ru and TaON layers were deposited on quartz plates after mask inspection. The Ru layer is used as the etch stop layer during defect formation. TaON layers of different thicknesses were deposited in four quadrants. Each quadrant had 1 nm, 2 nm, 4 nm, and 8 nm for different program defect depths or heights. The TaON layers were patterned by conventional e-beam writing, followed by resist coating, e-beam exposure, resist develop, dry etch, resist strip, and cleaning as shown in figure 3. Multilayers were deposited on top of the programmed defects under normal deposition conditions using an ion beam deposition (IBD) tool in SEMATECH's MBDC. The printability of defects strongly depends on the multilayer deposition conditions.[7] In this study, we compared printability characteristics using multilayers that were prepared under standard conditions. Defect dimensions were measured before and after multilayer deposition. The programmed defects were inspected at the AIT and analyzed using ThroughFocus software. To determine printability criteria, the intensity threshold of AIT intensity was set to 0.4, the choice of which is explained in another paper.[8]

Figure 4 shows the mask design for programmed defect formation. Eight identical boxes in each quadrant contain 16 different programmed defect arrays each. The dimensions of the 16 different patterns are shown in figure 5. Defects were 20 nm X 20 nm to 100 nm X 100 nm and 1 nm, 2 nm, 4 nm, and 8 nm deep. All dimensions of these program defects are on mask dimensions.

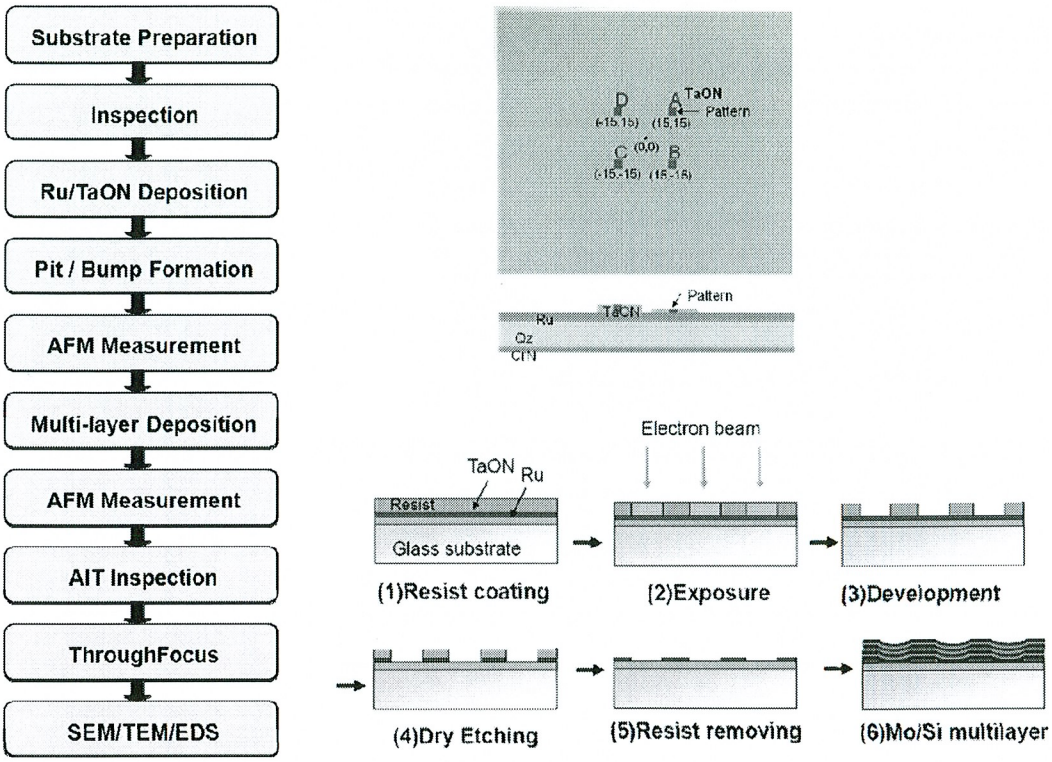

Figure 3. Experimental procedure for programmed defect mask preparation.

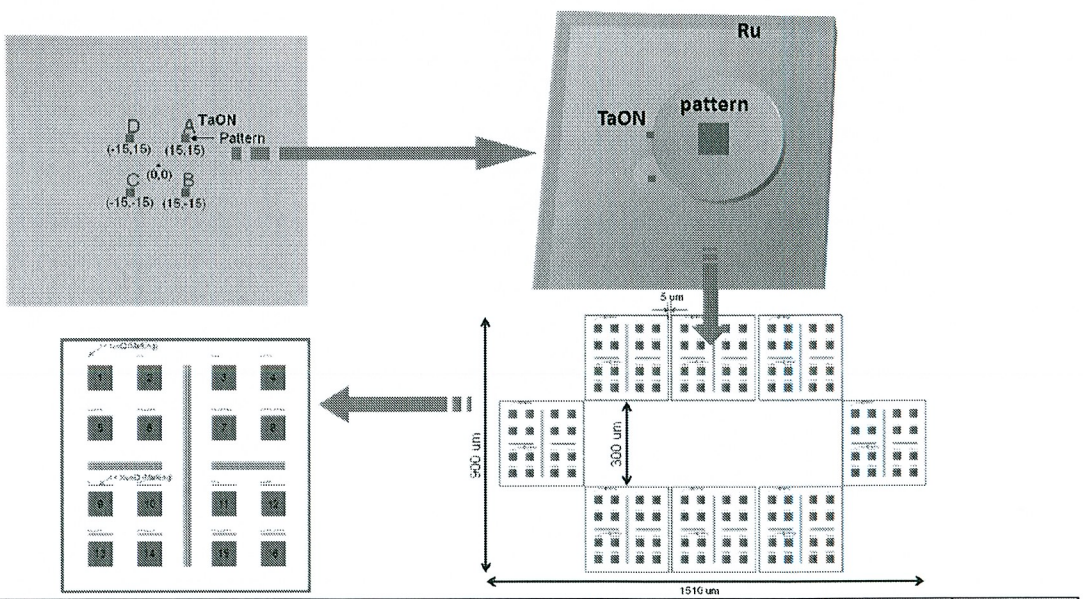

number	1	2	3	4	5	6	7	8
Area (nm)	20 × 20	30 × 30	40 × 40	50 × 50	60 × 60	70 × 70	80 × 80	100 × 100
number	9	10	11	12	13	14	15	16
Area (nm)	20 × 300	40 × 300	60 × 300	80 × 300	20 × 120	30 × 80	40 × 60	40 × 120

Figure 4. Pattern design for programmed defect masks.

3. RESULTS AND DISCUSSION

3.1 SEVD for defect printability

Some researchers are using sphere equivalent volume diameter (SEVD) to characterize defect dimensions. In our work, we analyzed the relationship between printed defects and SEVD, but found little correspondence[7] since SEVD is calculated from the dimensions on the top of the multilayer. As a result, even though the multilayer stack structures are different, the SEVD values from different defects can be the same. Figure 5 shows an example of this issue. Two native pit defects have different multilayer decoration characteristics, but the SEVDs of both defects are 31 nm. One defect is printed in the negative focus region and the other does not print in any region. SEVD can be used to investigate detectability, but not printability.

3.2 FWHM and height (depth) for printability

Figure 6 shows native bump defect printability characteristics in terms of full width at half maximum (FWHM) and height. Some of the printable and unprintable regions overlap. The FWHM and height are the dimensions on top of the multilayer without considering multilayer decoration characteristics. Consequently, we need to be very careful to use FWHM and height/depth to characterize printable and unprintable regions.

3.3 Multilayer damages for printability

Defects can be generated at the bottom or top of the multilayer during the multilayer deposition. Some defects are generated from the substrate and decorated during multilayer deposition. The dimensions at the top of the multilayer are unable to provide any printability information about defect decoration. Some defects are generated on top of the multilayer and detected by the inspection tool. We could not separate these different types of defects using pixels from the inspection tool and/or dimensions from AFM. Figure 7 shows another example of the defects. The top of the multilayer sustained some damage from cleaning; the printability of defects in these top layers is different from the defects that are decorated by the bottom of the multilayer. While these different behaviors were reported in a previous paper,[7] we could not access cross-sectional images at that time.

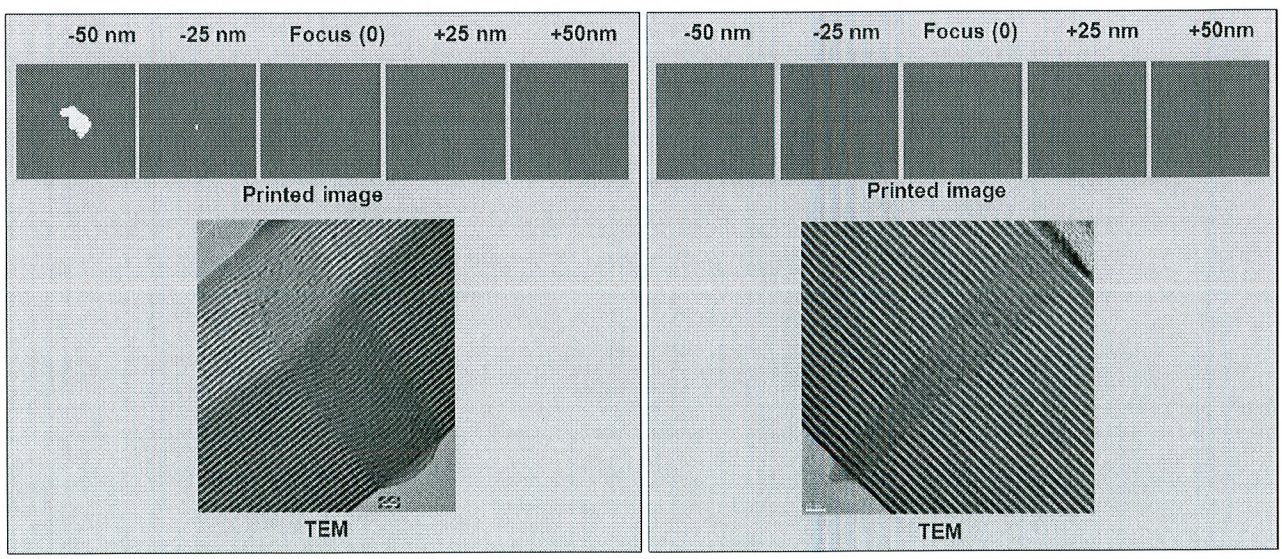

(a) (b)

Figure 5. Defect printability of native defects. Both defects have a SEVD of 31 nm. SEVD was calculated using FWHM and height from AFM data.

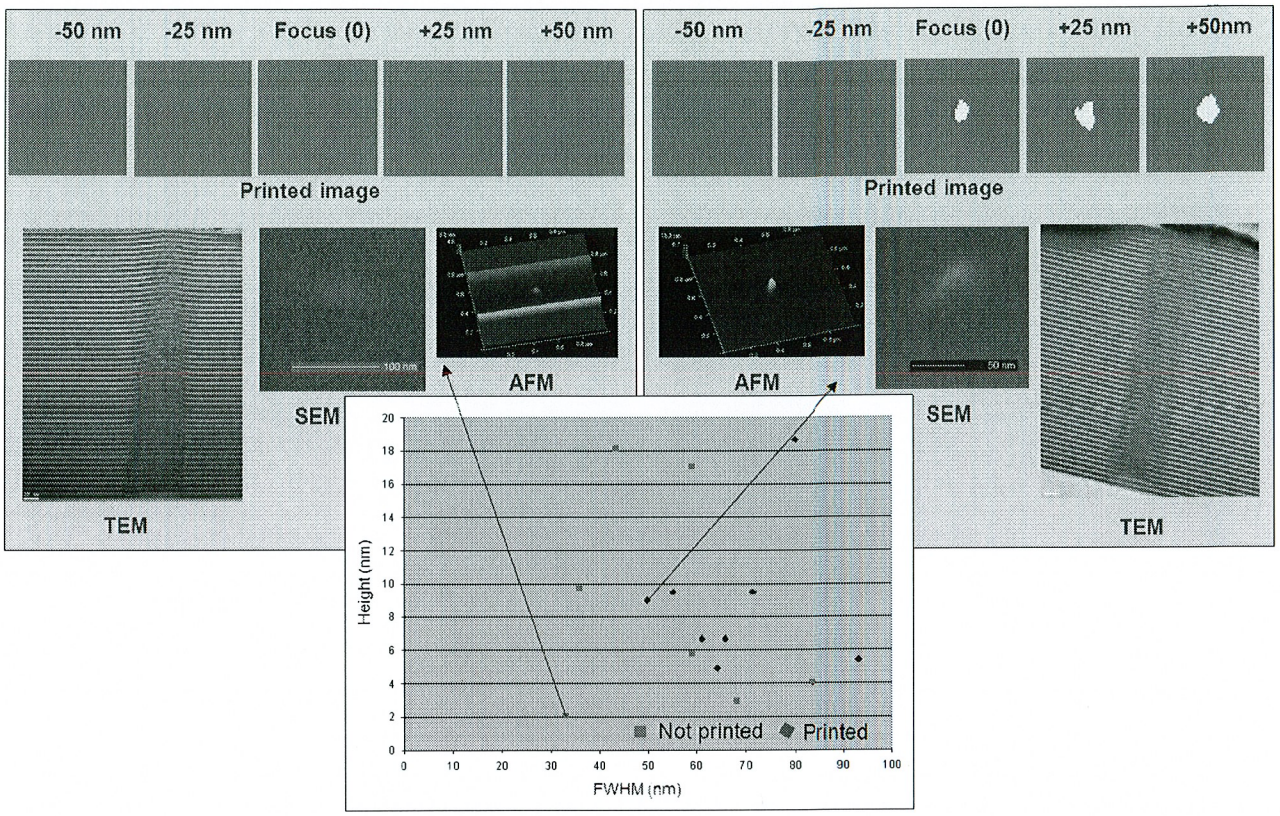

Figure 6. Native defect printability. FWHM and height were measured by AFM.

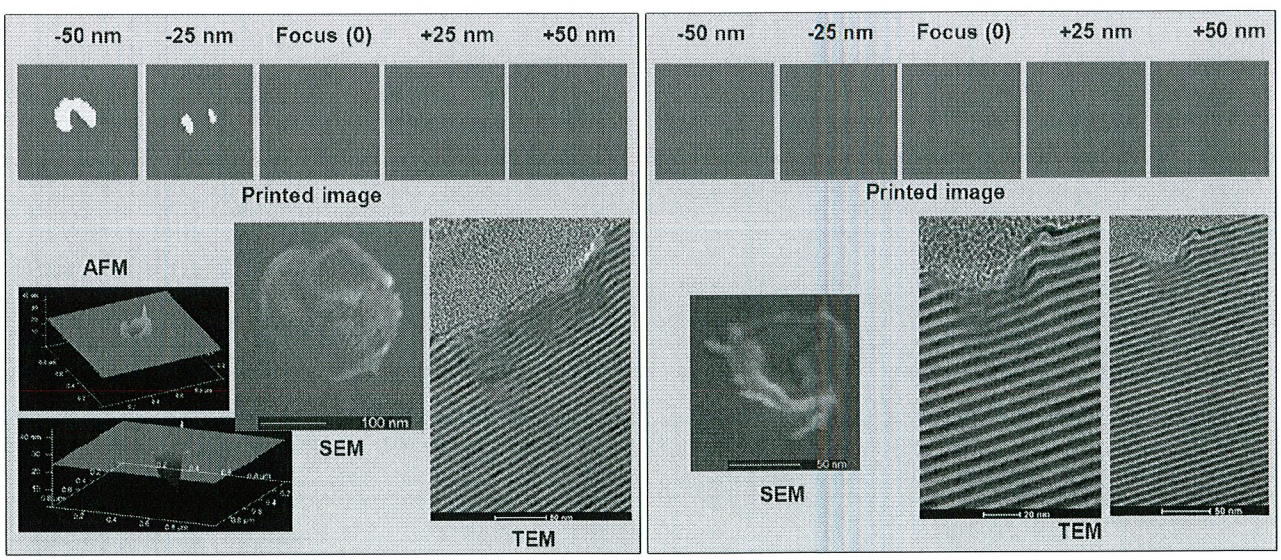

(a) (b)

Figure 7. Printability of damaged multilayer.

TEM images in figure 7 show the different printable and unprintable defects. Although we need to collect more images to draw more definitive conclusions about printability, tentatively we can conclude that native defects damaged with less than 6 multilayers and less than 80 nm wide do not print at a focus range of -50 nm to +50 nm. Native defects damaged with more than 12 multilayers with over 200 nm do print at -50 nm to +50 nm. We need to investigate more defects to determine the printed region and unprinted regions between these two regions.

3.4 Decoration for programmed defects

We deposited multilayers on top of the programmed defects using SEMATECH's standard conditions for multilayer deposition. The programmed defects were measured to determine their dimensions before and after deposition. Figure 8 compares pit depths at the bottom of the multilayer and at the top. Depths decreased by 63 percent after multilayer deposition under standard deposition conditions, but widths increased 21 nm on average.

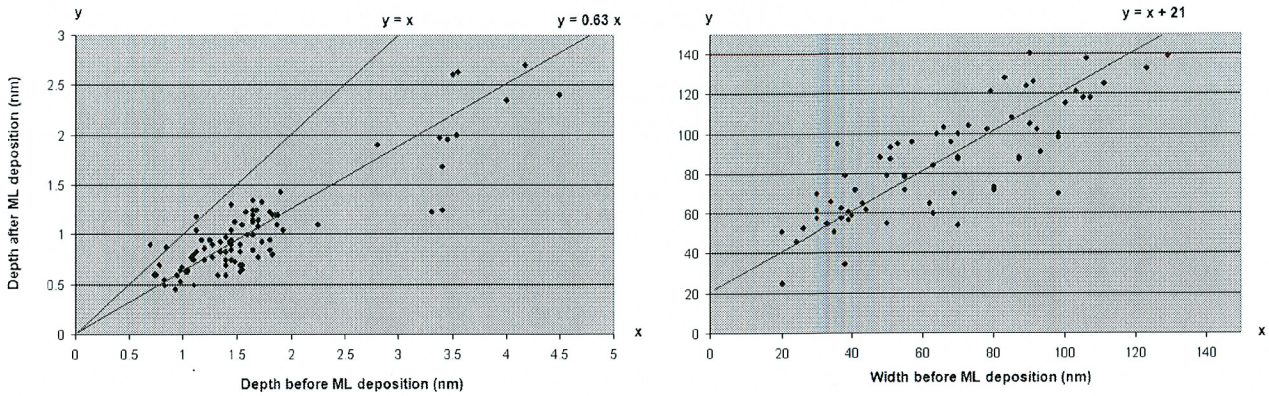

(a) (b)

Figure 8. Defect decoration of programmed defects. (a) Depth of programmed pit defects before and after multilayer deposition and (b) Width of programmed pit defects before and after multilayer deposition.

3.5 Programmed defect printability

The printability of programmed pit defects is shown in figure 9. The dimensions for FWHM and depth are at the bottom of the multilayer. When the focus range is -100 nm to +100 nm, there are overlapping areas of printable and unprintable regions as shown in figure 9(a). However, when the focus range is -50 nm to +50 nm as shown in figure 9(b), the printable and unprintable regions are separate. Most defects with a FWHM less than 70 nm and depth less than 1.5 nm do not print at the focus range of -50 nm to +50 nm.

The printability of pit programmed defects in relation to the top of the multilayer is shown in figure 10. Most defects less than 0.7 nm deep do not print at a focus range of -100 nm to +100 nm as shown in figure 10(a). When the focus range is -50 nm to +50 nm (figure 10(b)), most defects less than 0.8 nm deep do not print and most defects with a FWHM of less than 60 nm and depth less than 1.3 nm do not print. With the programmed defects, the printable regions are clearly distinguishable from unprintable regions.

3.6 Native defect printability

The printability of native phase defects is different from programmed phase defects as shown in figure 11. The printable and unprintable regions for native defects overlap, making it difficult to distinguish between them. This suggests that native defects become mishapen during multilayer deposition and that their shapes vary considerably. The cross-sectional TEM images in figures 5, 6, and 7 can give some clues to their printability behaviors. As shown in figures 9 and 10, the unprintable and printable regions for programmed defects are easier to see.

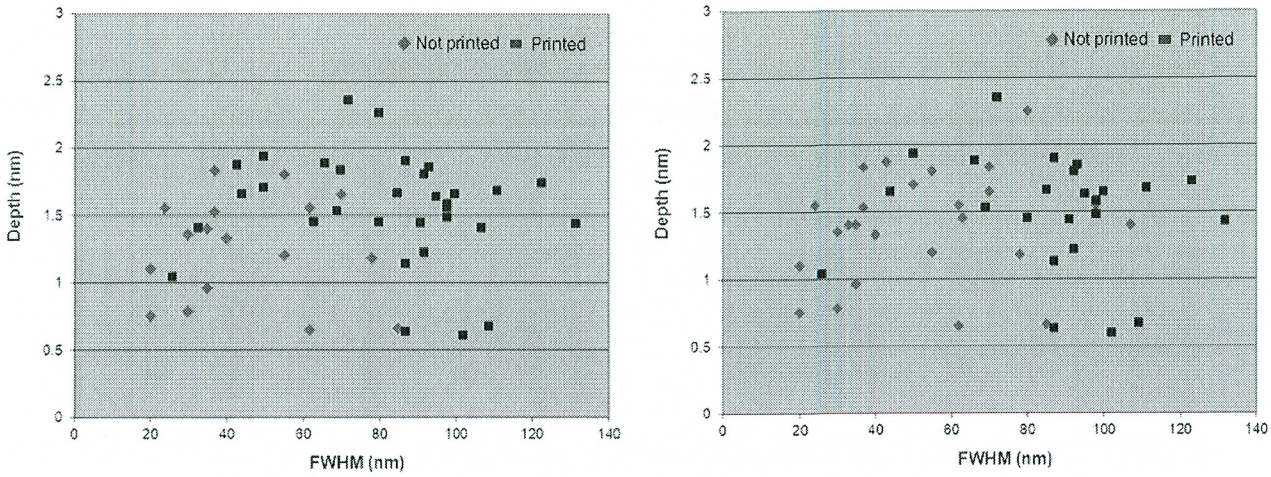

(a) (b)

Figure 9. Programmed defect printability. FWHM and depth were measured at the bottom of the multilayer. (a) Focus range printability is -100 nm to +100 nm and (b) Focus range printability is -50 nm to +50 nm.

The printability of programmed defects is more predictable than that of native defects. Knowing the printability characteristic of programmed defects, we can expect that most pit defects less than 0.8 nm deep will not print; however, we do not have enough data about native defects less than 0.8 nm deep to make a prediction. For defects more than 1 nm deep, programmed defects are more likely to print than native defects. Few programmed defects do not print if the pit is more than 1 nm deep. However, many native defects do not print even though they are deeper than 1 nm. Native defects are therefore more of a concern and should be evaluated with 3D images. This is a good reason to use an AIT for printability studies.

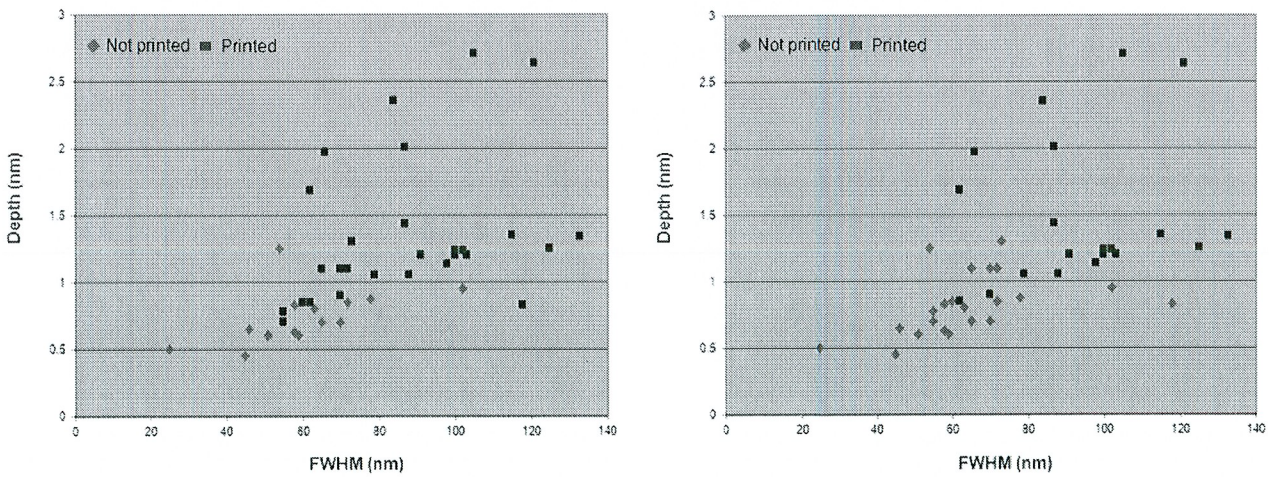

(a) (b)

Figure 10. Pattern design for programmed defects. FWHM and depth were measured at the top of the multilayer. (a) Focus range for printability is -100 nm to +100 nm and (b) Focus range for printability is -50 nm to +50 nm.

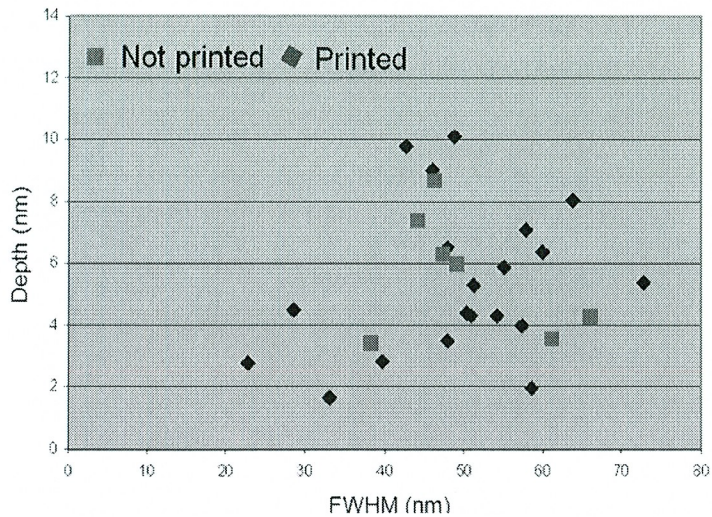

Figure 11. Native defect printability. The focus range for printability was -100 nm to +100 nm.

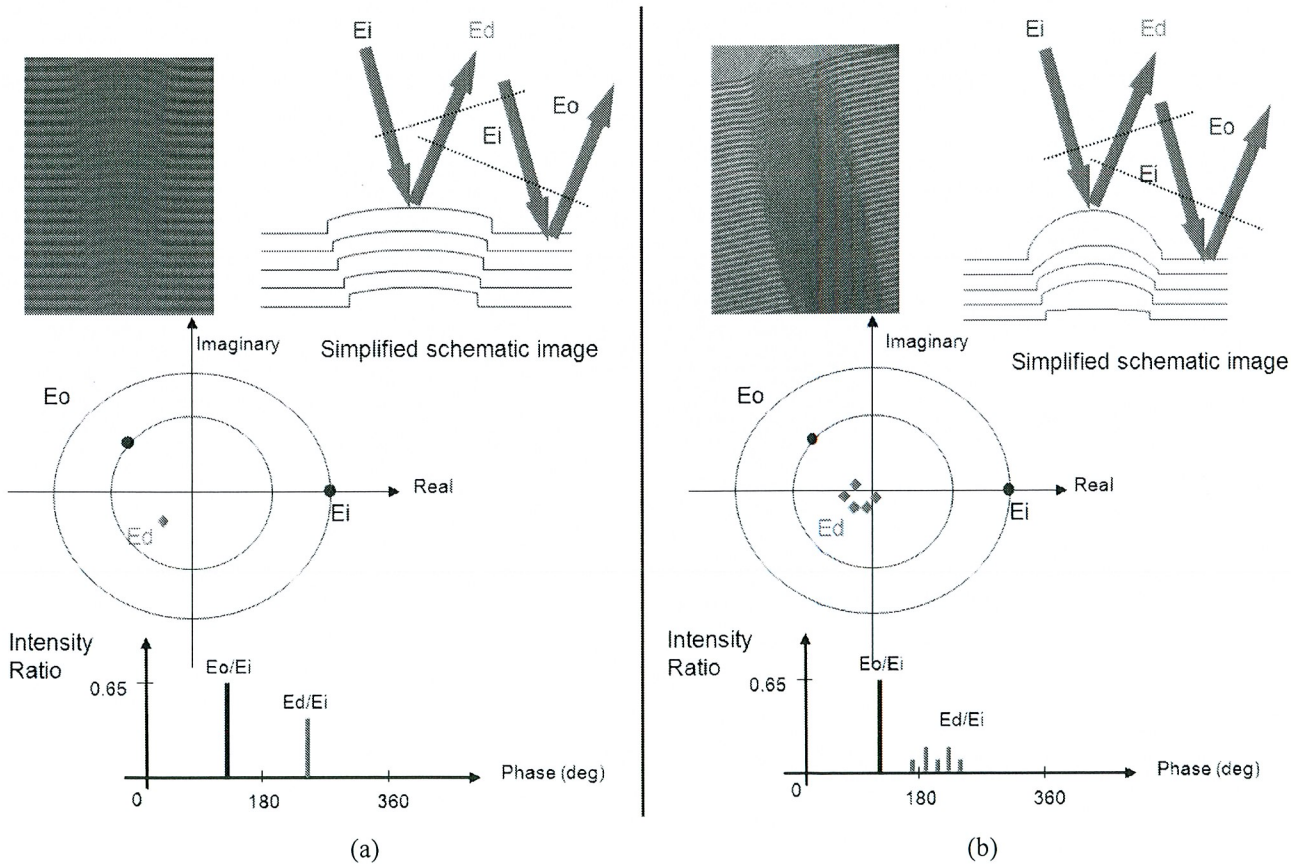

Figure 12. Simplified printability model. (a) High intensity with narrow phase range and (b) Low intensity with wide phase range.

3.7 Simplified printability model

Because a 3D structure is a critical parameter for printability, we need to consider the multilayer stack structure. We propose the simplified model shown figure 12[7] for analyzing printability. In figure 12(a), the multilayer was uniformly deposited on top of the defect in the multilayer stack. As shown in figure 12(b), however, the shape of the multilayer changes during deposition. The phase defect in figure 12(a) has a high intensity with a narrow phase range, but the defect in figure 12(b) has a low intensity with a wide phase range. The phase error for the defect in figure 12(a) is relatively uniform and the phase intensity is higher than that of the defect in figure 12(b). If the phase errors for the defects are out of phase range, the intensity of the defect in figure 12(a) is more likely to drop, rendering it more printable than the defect in figure 12(b). The multilayer decoration structure depends heavily on the multilayer deposition conditions as reported in a previous paper[7]; hence, we need to be careful when drawing general conclusions about printability characteristics. In our experiments using SEMATECH's standard multilayer deposition conditions with native and programmed defect, we nevertheless could determine sufficient printability characteristics to discern differences between native and programmed defects. Native defects are more likely to be deposited like the defect in figure 12(b), but programmed defects are more likely to be deposited like the defect in figure 12(a). When the conditions of multilayer deposition were altered, we needed a cross-sectional image to clarify which model the resultant multilayer structure followed.

4. SUMMARY

This study addressed mask blank defect printability using the AIT and comparisons of 3D images, including cross-sectional TEM images. Pixel, FWHM, depth, height, and/or SEVD cannot provide meaningful data about printability; therefore, the AIT was used to study printability. Printable and unprintable regions were found to be different for native defects and programmed defects. At small dimensions, programmed defects are more likely to print than native defects. We could not easily separate the printed and unprinted regions for native defects. The AIT and 3D data are needed to understand their printability behavior. We could find unprinted regions with programmed defects. The unprinted regions at the focus range of -50 nm ~ 50 nm are the substrate dimensions (below the multilayer) with the FWHM of less than 70 nm and depth less than 1.5 nm. The unprinted regions at the focus range of -50 nm ~ 50 nm are the multilayer top dimensions with a depth less than 0.8 nm or with a FWHM of less than 60 nm and depth less than 1.3 nm.

REFERENCES

[1] K. A. Goldberg, A. Barty, Y. Liu, P. Kearny, Y. Tezuka, T. Terasawa, J. S. Taylor, H. S. Han, and, O. R. Wood, "Actinic inspection of extreme ultraviolet programmed multilayer defects and cross-comparison measurements," J. Vac. Sci. Technol. B 24(6), 2824 (2006).

[2] T. Yamane, T. Iwasaki, T. Tanaka, T. Terasawa, O. Suga, T. Tomie, "Actinic EUVL mask blank inspection and phase defect characterization," Proc. SPIE 7379, 73790H (2009)

[3] S. Huh, L. Ren, D. Chan, S. Wurm, K. A. Goldberg, I. Mochi, T. Nakajima, M. Kishimoto, B. Ahn, I. Kang, J. Park, K. Cho, S. Han, and T. Laursen, "A study of defects on EUV masks using blank inspection, patterned mask inspection, and wafer inspection," Proc. SPIE 7636, 76360K (2010)

[4] I. Mochi, K. A. Goldberg, B. La Fontaine, A. Tchikoulaeva, and C. Holfeld, "Actinic imaging of native and programmed defects on a full-field mask," Proc. SPIE 7636, 76361A (2010)

[5] R. Jonckheere, D. Heuvel, T. Bret, T. Hofmann, J. Magana, I. Aharonson, D. Meshulach, E. Hendrickx, and K. Ronse, "Evidence of printing blank-related defects on EUV masks missed by blank inspection," Proc. SPIE 7985, 79850W (2011)

[6] K. A. Goldberg, I. Mochi, S. B. Rekawa, N. S. Smith, P. P. Naulleau and J. B. Macdougall, "An EUV Fresnel zoneplate mask-imaging microscope for lithography generations reaching 8 nm," Proc. SPIE 7969, 796910 (2011)

[7] H. J. Kwon, J. Harris-Jones, T. Ranganath, V. Jindal, D. Chan, F. Goodwin, "Native Blank Defect Analysis for the Study of Printability," EIPBN 2011, Las Vegas, (2011)

[8] S. Huh, A. Rastegar, S. Wurm, K. Goldberg, I. Mochi, T. Nakajima, M. Kishimoto, and M. Komakine, "Study of real defects on EUV blanks and a strategy for EUV mask inspection," Proc. SPIE 7545, 75450N (2010)

This work was supported by the Director, Office of Science, of the U.S. Department of Energy under Contract No. DE-AC02-05CH11231.